

# European Spallation Source as a searching tool for an ultralight scalar field

Rubén Cordero,<sup>1,\*</sup> Luis A. Delgadillo,<sup>1,†</sup> and O. G. Miranda<sup>2,‡</sup>

<sup>1</sup>*Departamento de Física, Escuela Superior de Física  
y Matemáticas del Instituto Politécnico Nacional,*

*Unidad Adolfo López Mateos, Edificio 9, 07738 Ciudad de México, Mexico*

<sup>2</sup>*Departamento de Física, Centro de Investigación y de Estudios*

*Avanzados del IPN Apdo. Postal 14-740 07000 Ciudad de México, Mexico*

Dark matter (DM) nature is one of the major issues in physics. The search for a DM candidate has motivated the known proposal of an ultralight scalar field (ULSF). We explore the possibility to search for this ULSF at the upcoming European Spallation Source neutrino Super-Beam experiment. We have considered the recent study case in which there could be an interaction between the ULSF and active neutrinos. We have found that in this future experimental setup, the sensitivity is competitive with other neutrino physics experiments. We show the expected future sensitivity for the main parameter modeling the interaction between ULSF and neutrinos.

---

\* [rcorderoe@ipn.mx](mailto:rcorderoe@ipn.mx)

† [ldelgadillof2100@alumno.ipn.mx](mailto:ldelgadillof2100@alumno.ipn.mx)

‡ [omar.miranda@cinvestav.mx](mailto:omar.miranda@cinvestav.mx)

## I. INTRODUCTION

The existence of dark matter (DM) is one of the most intriguing aspects of modern cosmology. Nearly one fourth of the matter-energy content of the Universe is in the form of dark matter and elucidating its nature is a very fundamental issue. There are plenty of proposals to model dark matter, from objects like primordial black holes with masses of the order of  $2 \times 10^{21}$  Kg ( $10^{57}$  eV/ $c^2$ ), weakly interacting massive particles (WIMPs) with masses around  $100$  TeV/ $c^2$ – $2$  GeV/ $c^2$ , axions with masses of  $10^{-5}$  eV/ $c^2$ , or ultralight scalar dark matter particles with masses of  $10^{-22}$  eV/ $c^2$ .

One of the proposals for a dark matter candidate postulates that an ultralight relativistic scalar field  $\phi$  can model dark matter with a suitable scalar potential  $V(\phi)$  [1–6] (see, for example, the following reviews [7–12]). The general property of this scalar field potential is the existence of a parabolic minimum around which it is possible to define a mass scale for the related boson particle. In this model, the galactic halos can be formed by condensing the scalar field at the Universe’s beginning [7]. The successful physical implications of  $\Lambda$ CDM at cosmological scales are replicated by the scalar field dark matter, e.g., the evolution of the cosmological densities [13], the acoustic peaks of the cosmic microwave background radiation (CMBR) [14], the rotations curves in big- and low-surface brightness (LSB) galaxies [15–18], and the observed properties of dwarf galaxies [19].

Besides, the oscillations of the scalar field could have exciting and important physical consequences. Since neutrinos have small masses, the interaction with the oscillations of the scalar field could have a relevant influence on neutrino masses and mixing. Considering that the mechanism of neutrino masses is still unknown, the interaction with the oscillating scalar field could provide a link to physics beyond the Standard Model (SM). The former reasons constitute a strong motivation to study the effects of a light scalar field in neutrino oscillations.

More recently, searches for an ultralight scalar field at neutrino oscillation experiments are becoming possible (see, e.g., Refs. [20–26]) due to advancements in the energy resolution of present and upcoming neutrino oscillation experiments. Besides, feasible cosmological models of active and/or sterile neutrinos interacting with an ultralight scalar field have been explored [27–31]. In Ref. [32], the implications for the reactor neutrino experiments Kamioka liquid-scintillator antineutrino detector (KamLAND) and Jiangmen Underground Neutrino

Observatory (JUNO) due to interactions between active neutrinos and a scalar field with mass  $m_\phi \gtrsim 10^{-12} \text{ eV}/c^2$  are considered. Despite these interesting studies, it is important to notice that such an interaction between neutrinos and the ultralight scalar field (ULSF) may also lead to tension with current experimental observables, as we will discuss below. Moreover, recent studies corner the ultralight dark matter (ULDM) proposal to be only a subdominant component of the DM content [33, 34]. Still, the interaction of a neutrino with a ULSF can be of interest independently of its connection to the DM problem.

In this paper, we will explore the phenomenological consequences of having an ultralight scalar field mixed with the neutrino mass eigenstates and the capabilities of an European Spallation Source Neutrino Super Beam (ESS $\nu$ SB)-like experiment [35–37] to constraint these interactions. The original proposal is to study a neutrino Super Beam, which employs the European Spallation Source (ESS) facility as a neutrino source with a water Cherenkov detector [38] located in a deep mine, for the discovery of the Dirac  $CP$ -violating phase  $\delta$ . We consider two baselines. One at 360 km, corresponding to the distance from the source to the Zinkgruvan mine. While the second would be at 540 km, with a detector placed at the Garpenberg mine; both mines are located in Sweden. Moreover, scenarios that investigate the capabilities of the ESS $\nu$ SB experiment to probe physics beyond the Standard Model and neutrino oscillations have been discussed [39–45].

The structure of the paper is as follows. In Sec. II, we present one possible form of interaction between neutrinos and the ultralight scalar field. This interaction modifies the leptonic mixing angle  $\theta$ , and adds a smearing on the neutrino mass squared difference  $\Delta m^2$ . Section III explains the characteristics and assumptions made in the general long baseline experiment simulator (GLOBES) software [46, 47] to simulate the ESS $\nu$ SB experiment. Sensitivities to the ULSF via modulations from average distorted neutrino oscillations are developed in Sec. IV. Finally, we give our conclusions.

## II. FRAMEWORK

The existence of dark matter has stimulated extensive and intensive activity to explain its characteristics. There are a plethora of possible candidates for dark matter. In this section, we will mention some of the more studied proposals. For example, primordial black holes could have been formed soon after the big bang from the gravitational collapse of

higher-density mass regions. Some constraints restrict the masses of primordial black holes to several windows between  $10^{13} - 10^{14}$  kg,  $10^{17} - 10^{21}$  kg, and  $10 - 10^3$  solar masses ( $2 \times 10^{30}$  kg) [48]. However, from latest results of LIGO and VIRGO, it seems that primordial black holes only provide some part of the needed amount of dark matter [49].

The main characteristics that must fulfill a possible particle candidate for dark matter are that it has to be stable over billions of years, nonrelativistic, massive, and weakly interacting. The Standard Model of particle physics does not have a particle with these properties.

One of the most studied extensions of the Standard Model is its minimal supersymmetric extension (MSSM) [50]; several candidates for WIMPs can emerge in this model. The possible candidates for dark matter are neutralinos, gravitinos, and sneutrinos. The neutralino is the most studied particle candidate for dark matter; it has been extensively searched at the LHC. In the LEP and Tevatron experiments, a lower-mass bound around  $46 \text{ GeV}/c^2$  has been set [50]. The gravitino couples very weakly to other particles; therefore, it is challenging to impose any constraint on it [50]. The lightest sneutrino is strongly interacting, which is unsuitable for a dark matter particle.

Another popular dark matter candidate is the axion, a light neutral particle that can be produced in the early Universe by a spontaneous symmetry breaking of  $U_a(1)$  Peccei-Quinn symmetry [50, 51]. Experimental attempts have been developed to detect the axions using the prediction that axions and photons could be transformed into each other in an intense magnetic field [52].

Besides the former candidates for dark matter, there are other massive particles like sterile neutrinos that only interact gravitationally, with masses around  $\mathcal{O}(\text{keV}/c^2)$  [53, 54].

Furthermore, other exotic dark matter candidates exist like WIMPzillas, strongly interacting massive particles (SIMPs), Q-nuggets, Q-balls, gluinos, Fermi balls, EW balls, GUT balls, etc. The masses of these objects range from  $100 \text{ GeV}/c^2$  to a  $\text{TeV}/c^2$  [52, 55].

Another approach consists of avoiding the existence of massive dark matter particles or objects and instead considering modifications of gravitational interactions, for example, modified newtonian dynamics (MOND) [56, 57] and extra dimensions [58, 59].

Regarding the scalar-field dark matter, there are some problems that this proposal can solve. For example, on the cosmological side there are problems with certain predictions of  $\Lambda\text{CDM}$  at the galactic scale. Some examples are the excess of substructures produced in  $N$ -body numerical simulations, which are one order of magnitude larger than the observed ones,

and the cusp profile of central density in galactic halos [60–62]. Additionally, problems arise in numerical simulations of structure formation, which do not produce pure disk galaxies, among other problems. The former problems could be avoided if the structure grew faster than in  $\Lambda$ CDM [63].

Some of the former problems are resolved in the ultralight relativistic scalar field framework. In this model, the galactic halos are formed by a Bose-Einstein condensation of a scalar boson with a mass around  $m_\phi \sim 10^{-22} \text{ eV}/c^2$ .

The Compton length associated with this boson is of the order of kpc, which is the same order as the size of dark halos in typical galaxies. It is proposed that the dark halos are very big drops of scalar field. Then, when the Universe reaches the critical temperature of condensation, all galactic halos form at the same time producing well-formed halo galaxies at high  $z$ , which is a different prediction from  $\Lambda$ CDM [19].

The scalar field dark matter can resolve the problem of cusp profile of density in galactic halos since this is avoided due to the wave properties of the ultralight mass of the scalar particles [2, 64]. Furthermore, the excess of substructures is prevented by considering that the scalar field has a natural cutoff [2, 65, 66].

Although we consider here a scalar boson mass,  $m_\phi \sim 10^{-22} \text{ eV}/c^2$ , it is important to mention that this value can change from different physical constraints and different astrophysical models. Except for some few models [67, 68], all the justification for this mass region comes from consistency with astrophysical observations. For example, from the anisotropies of the CMB, the mass of the scalar field could be in the range of  $m_\phi = 10^{-24} - 10^{-22} \text{ eV}/c^2$  [12]. From galaxy rotation curves, the ULDM mass lies in the region  $m_\phi = 0.5 \times 10^{-23} - 10^{-21} \text{ eV}/c^2$  [69, 70].

In addition, it is expected that the ULDM cannot be the total fraction of the dark matter if the mass is light enough, although the exact value might be model dependent. For instance, the combined analysis of CBM and large-scale structure (LSS) data sets [71] allow ULDM masses  $m_\phi \gtrsim 10^{-24} \text{ eV}/c^2$  if  $\rho_\phi \sim \rho_{\text{DM}}$  and as low as  $m_\phi \sim 10^{-27} \text{ eV}/c^2$  if  $\rho_\phi \sim 0.05\rho_{\text{DM}}$ . Lyman- $\alpha$  forest excludes ULDM masses lighter than  $m_\phi \lesssim 10^{-21} \text{ eV}/c^2$  if  $\rho_\phi \sim \rho_{\text{DM}}$  while a ULDM mass  $m_\phi \sim 10^{-22} \text{ eV}/c^2$  can be accommodated if  $\rho_\phi \lesssim 0.2\rho_{\text{DM}}$  [33]. On the other hand, from the soliton-halo relation, a ULDM with mass below  $m_\phi \sim 10^{-21} \text{ eV}/c^2$  is disfavored [72]. Moreover, Ref. [34] suggests that the ULSF is not the total component of cosmological DM, if the mass range is  $10^{-24} \lesssim m_\phi (\text{eV}/c^2) \lesssim 10^{-20}$ , while admitting it

for  $\rho_\phi \lesssim 0.3\rho_{\text{DM}}$ . Finally, constraints from structure formation [73] exclude ULDM masses lighter than  $m_\phi \sim 10^{-20}$  eV/ $c^2$  if  $\rho_\phi \sim \rho_{\text{DM}}$  while the bound disappears when  $\rho_\phi \lesssim 0.1\rho_{\text{DM}}$ .

Let us review some of the main characteristics of the scalar field framework, which are relevant to our work. From the Lagrangian density for the scalar field

$$\mathcal{L} = \frac{1}{2}\nabla_\mu\phi\nabla^\mu\phi + V(\phi), \quad (1)$$

the conservation of the energy-momentum tensor  $\nabla_\mu T^{\mu\nu} = 0$  in the cosmological background of the Friedmann-Lemaître-Robertson-Walker metric gives

$$\ddot{\phi} + 3H\dot{\phi} + V'(\phi) = 0, \quad (2)$$

where  $H = \dot{a}/a$  is the Hubble parameter and  $a$  is the scale factor of the Universe. In the following, we will use natural units where  $c = \hbar = 1$ . The scalar energy density is [7]

$$T_0^0 = \frac{1}{2}\dot{\phi}^2 + V(\phi) = \rho_\phi.$$

The evolution of the scalar field can be obtained numerically near the minimum of the potential where  $V'(\phi) = m_\phi^2\phi$ . The contribution from the other components of matter-energy density present in the Universe is included in the Friedmann equation

$$H^2 = \frac{8\pi G}{3}(\rho_r + \rho_m + \rho_\phi + \rho_\Lambda), \quad (3)$$

and  $\rho_r$ ,  $\rho_m$ , and  $\rho_\Lambda$  are the energy densities associated with radiation, baryonic nonrelativistic matter, and dark energy, respectively. However, there are analytical approximations for the scalar fields in recent times when  $H_0 \sim 10^{-33}$  eV and  $H_0 \ll m_\phi$ . It has been proposed [7] the following ansatz for the scalar field

$$\phi = 2\sqrt{\hat{\rho}}\cos(S - m_\phi t). \quad (4)$$

In late times, the scalar field behaves as nonrelativistic, and the relation  $\dot{S}/m_\phi \sim 0$  is fulfilled when the temperature at which the scalar field begins to oscillate is  $T_{\text{osc}} \sim \text{keV}$  corresponding to a redshift  $z_{\text{osc}} \sim 10^6$  [10] if  $m_\phi \sim 10^{-22}$  eV.

From the evolution equation for the scalar field Eq. (2),  $\hat{\rho} = \hat{\rho}_0 a^{-3}$  is obtained, which is proportional to the energy density of non-relativistic matter. From the expression of the scalar-field energy density, it is possible to obtain  $\rho_\phi = 2m_\phi^2\hat{\rho}$ . The ultralight scalar field can be described by a classical field minimally coupled to gravity [74]. For instance, by setting

the phase  $S = \pi/2$  and writing the scalar field in terms of the energy density, we can have a ULSF that oscillates with time as

$$\phi \simeq \phi_0 \sin(m_\phi t), \quad (5)$$

with  $m_\phi \sim 10^{-22}$  eV and

$$\phi_0 \simeq \frac{\sqrt{2\rho_\phi}}{m_\phi}, \quad (6)$$

where  $\rho_\phi$  is the field density at the surface of the Earth, which we will assume to be  $0.3 \text{ GeV/cm}^3$ ,  $\rho_\phi \leq \rho_{\text{DM},\odot} = 0.3 \text{ GeV/cm}^3$ . From recent analyses, the estimation of the local DM density coincide within a range of  $\rho_{\text{DM},\odot} \simeq 0.3 - 0.6 \text{ GeV/cm}^3$  [75–77].

If we consider that this scalar field can interact with the neutrino, a modification in the leptonic mixing angle  $\theta$  or additional smearing on the neutrino mass-squared difference  $\Delta m^2$  will arise. Recently, the possible interaction between the ULSF and neutrinos and its implications have been considered [20, 25, 26, 28]. In this case, the ULSF can produce an effect on neutrino oscillations. Besides the SM Lagrangian, we would have an additional contribution due to the hypothetical ULSF interaction with the neutrino [20, 26]

$$\mathcal{L}_{\lambda,y} \supset \frac{\lambda^{\alpha\beta}}{\Lambda} (L_\alpha)^T L_\beta H H + \frac{y^{\alpha\beta}}{\Lambda^2} \phi (L_\alpha)^T L_\beta H H, \quad (7)$$

where  $\lambda^{\alpha\beta}$  and  $y^{\alpha\beta}$  are  $3 \times 3$  dimensionless symmetric matrices, and  $\Lambda$  is the scale of new physics.

$$\mathcal{L}_{m_\nu} \supset \frac{\lambda^{\alpha\beta} v^2}{2\Lambda} (\nu_\alpha)^T \nu_\beta + \frac{y^{\alpha\beta} v^2}{2\Lambda^2} \phi (\nu_\alpha)^T \nu_\beta. \quad (8)$$

After symmetry breaking and replacement of the Higgs field  $H$  by its vacuum expectation value  $\langle H \rangle = 1/\sqrt{2} (0, v)^T$ , the neutrino mass matrix acquires corrections from the ULSF field  $\phi$ :

$$\tilde{m} = m_\nu + \hat{y}\phi; \quad m_\nu = \frac{\lambda v^2}{\Lambda} \quad \text{and} \quad \hat{y} = \frac{y v^2}{\Lambda^2}. \quad (9)$$

For instance, the interaction term in Eqs. (7) and (8) can arise within the framework of a type I seesaw [22].

If we consider the off-diagonal  $\hat{y}$  matrix elements, we will obtain a correction to the leptonic mixing angle. In a  $2 \times 2$  neutrino picture, the mixing matrix for this case will have the form

$$\tilde{m} = m_\nu + \hat{y}\phi = \begin{pmatrix} m_1 & \hat{y}_{12}\phi \\ \hat{y}_{12}\phi & m_2 \end{pmatrix}. \quad (10)$$

To diagonalize this matrix, we can apply a rotation,  $R(\psi)$ , such that  $\tan(2\psi) = -\hat{y}_{12}\phi/\Delta m$ . For small angles,  $\psi$ ,  $\tan(2\psi) \approx 2\psi$  and  $\psi \approx -\hat{y}_{12}\phi/\Delta m$ . Once the mass matrix is diagonal, we can rotate to the flavor basis through a new transformation  $R(\theta)$ . Since  $R(\theta)R(\psi) = R(\theta + \psi)$ , then, the mixing angle receives contributions from the  $\hat{y}_{12}$  term, such that  $\tilde{\theta} \rightarrow \theta + \hat{y}_{12}\phi/\Delta m$ ,  $\tilde{\theta} \rightarrow \theta + \eta_\theta \sin m_\phi t$ . However, our sensitivity, in this case, will be limited. Therefore, we will concentrate on the case of diagonal couplings.

In the case of two neutrino mixing, if we consider only diagonal couplings ( $\alpha = \beta$ ), the modified  $\hat{y}$  matrix up to leading order is

$$\tilde{m}^2 = (m_\nu + \hat{y}\phi)^2 \simeq \begin{pmatrix} m_1^2 + 2m_1\hat{y}_{11}\phi & 0 \\ 0 & m_2^2 + 2m_2\hat{y}_{22}\phi \end{pmatrix} + \mathcal{O}(\hat{y}^2\phi^2). \quad (11)$$

Therefore, for the mass squared difference, we will have

$$\Delta\tilde{m}_{21}^2 \simeq m_2^2 - m_1^2 + 2(m_2\hat{y}_{22} - m_1\hat{y}_{11})\phi. \quad (12)$$

or

$$\Delta\tilde{m}_{21}^2 = \Delta m_{21}^2 \left[ 1 + \frac{2(m_2\hat{y}_{22} - m_1\hat{y}_{11})\phi}{\Delta m_{21}^2} \right] + \mathcal{O}(\hat{y}^2\phi^2) = \Delta m_{21}^2 \left[ 1 + 2\eta_\Delta \sin(m_\phi t) \right] + \mathcal{O}(\hat{y}^2\phi^2). \quad (13)$$

Furthermore, the ULSF parameter  $\eta_\Delta$  is given by

$$\eta_\Delta = \frac{(m_j\hat{y}_j - m_i\hat{y}_i)\sqrt{2\rho_\phi}}{\Delta m_{ji}^2 m_\phi} \quad (i < j). \quad (14)$$

Then, we can have a modification to the neutrino conversion probability due to the shift in the neutrino mass diagonal terms,

$$P_{\mu e} \simeq \sin^2 2\theta \sin^2 \left[ \frac{\Delta m^2 L}{4E_\nu} (1 + 2\eta_\Delta \sin(m_\phi t)) \right]. \quad (15)$$

In the next section, we will implement the simulation of the effects of scalar field diagonal couplings in neutrino oscillations.

### III. SIMULATION

The ESS linac is projected to be fully operational at 5 MW average power with an expected 2.5 GeV proton beam currently under construction in Lund, Sweden. It will be an essential user facility providing slow neutrons for research laboratories and the industry.



More importantly, for this study is the ESS $\nu$ SB initiative. A neutrino super-beam facility that will benefit from the ESS production of neutrons to search for the leptonic Dirac  $CP$ -violating phase  $\delta$  [35–37]; the data taking it is planned to start by 2035. It will investigate neutrino oscillations around the second oscillation maximum with two baselines in consideration at either 360 km or 540 km from the source. In addition to measuring the leptonic Dirac  $CP$ -violating phase, the ESS $\nu$ SB facility may be employed to detect cosmological neutrinos and neutrinos from supernova events and measure the proton lifetime.

This section presents the characteristics and assumptions performed in our study. We use GLoBES [46, 47] to simulate an ESS $\nu$ SB-like experiment with a 538 kt water Cherenkov detector [38]. The information on the neutrino fluxes is taken from Fig. 3 of the original proposal [35], which corresponds to a 2.0 GeV proton beam with  $2.7 \times 10^{23}$  protons on target per year <sup>1</sup> fixed at 5MW. Furthermore, the neutrino fluxes have been properly rescaled to the corresponding baseline at  $L = 360$  km, or  $L = 540$  km distance, as well as renormalized to the more recent simulation with 2.5 GeV proton kinetic energy [36]. The cross sections and efficiencies in the detector follow the specifications from Ref. [78]. We assume an energy resolution which follows a Gaussian distribution, with a width of  $\sigma(E) = 12\%/\sqrt{E[\text{GeV}]}$  for electrons and  $\sigma(E) = 10\%/\sqrt{E[\text{GeV}]}$  for muons, respectively. A total of 12 bins uniformly distributed in the energy interval of 0.1-1.3 GeV were considered. Moreover, a 10-year exposure on a far detector is considered in the form of 5 years in neutrino mode and 5 years in antineutrino mode. Nevertheless, in our calibration of the expected number of signal and background events, we have assumed a one-year exposure to match the results from the updated analysis released by the ESS $\nu$ SB collaboration [36]. Unless otherwise specified, the systematic errors are implemented as 10% signal normalization error and 15% background normalization error for both appearance and disappearance channels. In Refs. [35, 36], the systematic errors have been considered to be 5% (10%) for signal (background), respectively. Ours are more conservative. Furthermore, a 0.01% energy calibration error has been adopted for both types of events. Our event rates reasonably reproduce <sup>2</sup> the events reported in Tables 2 and 3 of Ref. [36].

<sup>1</sup> The annual operation period will be 208 days.

<sup>2</sup> Lately, the conceptual design report (CDR) for the ESS $\nu$ SB experiment was released [37]. From Table 8.1 of the CDR, an  $\mathcal{O}(10\%)$  improvement on the expected background events with respect to our simulation was demonstrated. Signal events remain in good agreement, as shown in Table [I]. As a result of our conservative assumptions, we do not expect considerable differences in our analysis.

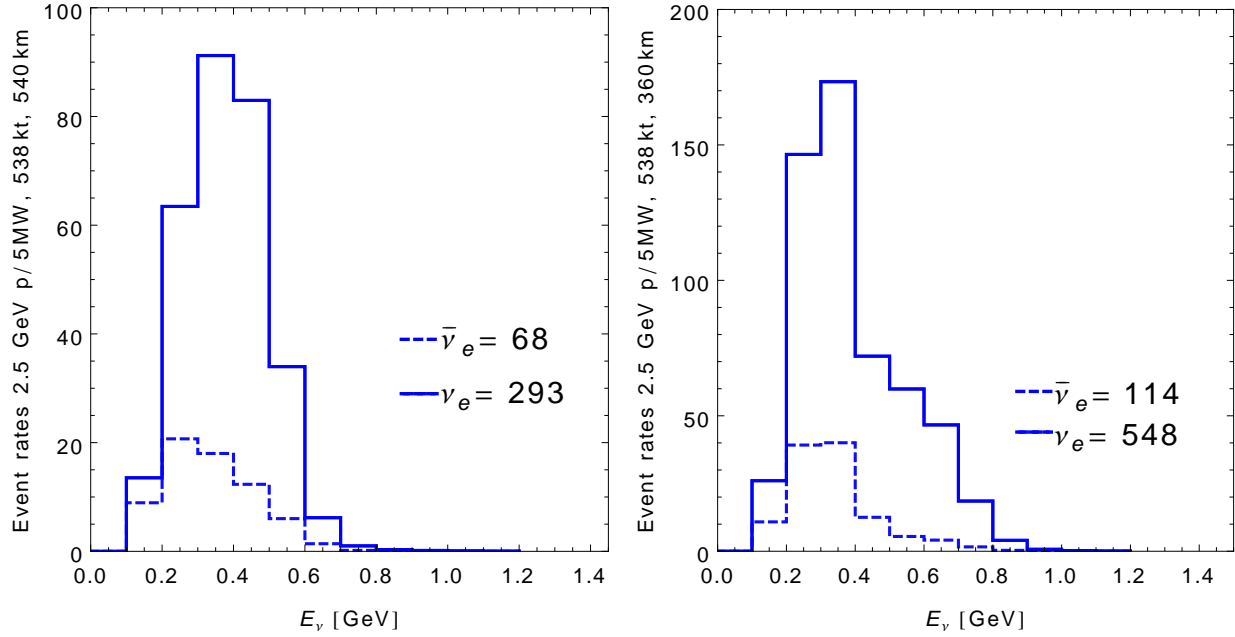


Figure 1: Expected electron-neutrino and antineutrino appearance ( $\nu_e/\bar{\nu}_e$ ) event rates per year for an ESS $\nu$ SB setup using the neutrino oscillation parameters as given in [36], the left panel displays the option of placing the detector at a baseline distance of  $L = 540$  km and the right panel for the  $L = 360$  km baseline case.

In Fig. 1, we display our expected signal events as a function of the neutrino energy, assuming one year of exposure for both neutrinos and antineutrinos. The left panel shows the case of a detector at a 540 km baseline from the source, and the right panel considers a 360 km baseline.

Baseline run	$\nu_e(\bar{\nu}_e)$ sig.	$\nu_\mu(\bar{\nu}_\mu)$ misidentified ID	$\nu_e$ beam	$\bar{\nu}_e$ beam	NC bckg.	$\bar{\nu}_\mu(\nu_\mu) \rightarrow \bar{\nu}_e(\nu_e)$
360 km $\nu$	548	87	164	0.2	37	3
( $\bar{\nu}$ )	114	19	3	26	5	9
540 km $\nu$	293	30	78	1	20	2
( $\bar{\nu}$ )	68	6	1	12	4	6

Table I: Our expected electron-neutrino appearance signal and background events per year for an ESS $\nu$ SB setup using the neutrino oscillation parameters as given in [36].

In Table I, our total number of events per year for both signal and background in the elec-

tron neutrino appearance channel are presented accordingly for neutrinos and antineutrinos. We have verified that with the inclusion of both electron and muon neutrino data sets (Tables I and II), our simulation accurately replicates the precision studies on the atmospheric mixing angle  $\theta_{23}$  and mass squared splitting  $\Delta m_{31}^2$  from Fig. 8 of the ESS $\nu$ SB Collaboration analysis [36]. Once we have established our experimental simulation and calibration of the number of events, in the following section, we proceed to describe the characteristics of our study.

#### IV. MODULATIONS FROM AVERAGE DISTORTED NEUTRINO OSCILLATIONS

In this section, we consider modulations of the ultralight scalar field in the regime  $\tau_\nu \ll \tau_\phi \ll \tau_{\text{exp}}$  (average distorted neutrino oscillations). Here,  $[\tau_\nu = (L/c)]$  is the neutrino time of flight,  $[\tau_\phi = 0.41 \times (10^{-14} \text{ eV}/m_\phi) \text{ seconds}]$  [25] is the characteristic modulation period of the scalar field and  $[\tau_{\text{exp}}]$  is the lifetime of the experiment. Under these circumstances, the oscillation effects from mixing angles or mass splittings are too quick to be observed, but an averaging effect on oscillation probabilities can be searched for [20, 22, 25, 26].

Regarding the scalar field mass sensitivities at the ESS $\nu$ SB facility, for the baseline choices,  $L = 540 \text{ km}$  and  $L = 360 \text{ km}$ , the corresponding neutrino times of flight are  $\tau_\nu^{540} \approx 1.8 \times 10^{-3} \text{ sec}$  and  $\tau_\nu^{360} \approx 1.2 \times 10^{-3} \text{ sec}$ , respectively. The total exposure of the experiment is  $\tau_{\text{exp}} = 10 \text{ years}$ . Therefore, for a ULSF modulation period  $\tau_\phi \approx 1 \text{ year}$ , we expect an ultralight scalar field mass sensitivity between  $2.0 \times 10^{-23} \text{ eV} \leq m_\phi^{540} \leq 1.3 \times 10^{-14} \text{ eV}$  and  $2.0 \times 10^{-23} \text{ eV} \leq m_\phi^{360} \leq 8.5 \times 10^{-15} \text{ eV}$ , respectively.

The original proposal of the ESS $\nu$ SB experiment [35] is to search and optimize the physics potential of leptonic Dirac  $CP$ -violating phase  $\delta$  around the second oscillation maximum. For this purpose, the electron neutrino appearance channel is the natural choice for performing the study. Despite its advantages for  $CP$ -violating phase searches, working with this channel in the second oscillation maximum implies limited statistics [79]. Therefore, in our case, the electron neutrino appearance channel might not be the optimal choice to hunt for ultralight scalar field. Thus we will perform a combined appearance and disappearance sensitivity study. In what follows, we will describe the central features of this analysis and its results.

### A. Electron-neutrino appearance channel

In this part of the analysis, we describe the phenomenology to search for a scalar field interaction with neutrinos via the ULSF parameter  $\eta$  in the electron neutrino appearance channel. We consider two proposed baseline distances, namely  $L = 360$  km and  $L = 540$  km corresponding to the upcoming ESS $\nu$ SB facility located in Sweden, under the regime of average distorted neutrino oscillations from the atmospheric mass squared difference  $\Delta m_{31}^2$ . Hence, the effect of the ULSF interaction in the  $P_{\mu e}$  oscillation probability for the two flavor approximation in vacuum is given by

$$P_{\mu e} \simeq \sin^2(2\theta_{23}) \left\langle \sin^2 \left( \frac{\Delta \tilde{m}_{31}^2 L}{4E_\nu} \right) \right\rangle, \quad (16)$$

with  $\Delta \tilde{m}_{31}^2 = \Delta m_{31}^2 [1 + 2\eta \sin(m_\phi t)]$ ; the average over the mass squared difference is given by [22, 25, 26]

$$\begin{aligned} \left\langle \sin^2 \left( \frac{\Delta \tilde{m}_{31}^2 L}{4E_\nu} \right) \right\rangle &= \frac{1}{\tau_\phi} \int_0^{\tau_\phi} dt \sin^2 [\Delta_{31} (1 + 2\eta \sin(m_\phi t))] \\ &\simeq \sin^2(\Delta_{31}) + 2 \cos(2\Delta_{31}) \Delta_{31}^2 \eta^2 + \mathcal{O}(\Delta_{31}^2 \eta^2)^2, \end{aligned} \quad (17)$$

where  $\tau_\phi$  is the ULSF period and  $\Delta_{31} = \frac{\Delta m_{31}^2 L}{4E_\nu}$ . More generally, the oscillation probability in the appearance channel considering matter effects used in this study follows from [80]:

$$\begin{aligned} P(\nu_\mu \rightarrow \nu_e) &= \sin^2 \theta_{23} \sin^2 2\theta_{13} \frac{\sin^2(\Delta_{31} - aL)}{(\Delta_{31} - aL)^2} \Delta_{31}^2 \\ &\quad + \sin 2\theta_{23} \sin 2\theta_{13} \sin 2\theta_{12} \frac{\sin(\Delta_{31} - aL)}{(\Delta_{31} - aL)} \Delta_{31} \frac{\sin(aL)}{(aL)} \Delta_{21} \cos(\Delta_{31} + \delta) \\ &\quad + \cos^2 \theta_{23} \sin^2 2\theta_{12} \frac{\sin^2(aL)}{(aL)^2} \Delta_{21}^2, \end{aligned} \quad (18)$$

where  $a = G_F N_e / \sqrt{2}$  is the matter potential,  $G_F$  is the Fermi constant,  $N_e$  is the electron density, and  $\Delta_{ij} = \Delta m_{ij}^2 L / 4E_\nu$ . For antineutrinos, we replace  $a \rightarrow -a$  and  $\delta \rightarrow -\delta$ . Furthermore, in this channel, the scalar field parameter,  $\eta$ , appears in the form of an average over the frequency of oscillations uniquely mediated by the atmospheric mass squared splitting  $\Delta m_{31}^2$  as shown in Eq. (17). The details on the expected signal and background events for this channel were discussed in the previous section Sec. III. As far as neutrino oscillation parameters are concerned, the true values used in this analysis are  $\Delta m_{21}^2 = 7.5 \times 10^{-5} \text{ eV}^2$ ,

$\Delta m_{31}^2 = 2.55 \times 10^{-3} \text{ eV}^2$ ,  $\theta_{12} = 34.3^\circ$ ,  $\theta_{13} = 8.53^\circ$ ,  $\theta_{23} = 49.26^\circ$ , and  $\delta = 194^\circ$ , corresponding to the best-fit values for normal ordering from Salas *et al.* [81].<sup>3</sup> For oscillation parameter priors, we assume a  $1\sigma$  error of 5% for  $\Delta m_{21}^2$ ,  $\Delta m_{31}^2$ ,  $\theta_{12}$ , and  $\theta_{23}$ . We also assume 3% for  $\theta_{13}$  and 10% for the leptonic  $CP$ -violating phase  $\delta$  [35]. In addition, matter effects were considered, for both baselines, with a constant density of  $\rho = 2.8 \text{ g/cm}^3$  [25].

## B. Muon-neutrino disappearance channel

Here we shift our attention to the muon-neutrino disappearance channel, which benefits from a larger event signal with minimal background contamination [36],<sup>4</sup> as displayed in Table II. Besides the agreement on the expected signal and background events, we verify that our simulation accurately replicates the precision studies on the atmospheric mixing angle  $\theta_{23}$  and mass squared splitting  $\Delta m_{31}^2$  from Fig. 8 of the ESS $\nu$ SB Collaboration analysis [36]. The muon -neutrino disappearance channel is optimal for investigating the ULSF oscillation phenomenology. We include in our analysis the corresponding matter effects needed for a complete study of the ESS case [83], although it does not significantly improve the sensitivity to  $\Delta m_{31}^2$  in our study, see e.g., the authors of Refs. [79, 83, 84]. In the standard oscillation case, neglecting  $\Delta m_{21}^2$  effects, the survival probability will be given by [85]

$$\begin{aligned}
 P(\nu_\mu \rightarrow \nu_\mu) \approx & 1 - \sin^2 \theta_{13}^M \sin^2 2\theta_{23} \sin^2 \left[ \frac{1}{2}(\Delta_{31} - \Delta_{31}^M + \Delta_A) \right] \\
 & - \cos^2 \theta_{13}^M \sin^2 2\theta_{23} \sin^2 \left[ \frac{1}{2}(\Delta_{31} + \Delta_{31}^M + \Delta_A) \right] \\
 & - \sin^2 2\theta_{13}^M \sin^4 \theta_{23} \sin^2 \Delta_{31}^M,
 \end{aligned} \tag{19}$$

where  $\Delta_{31}^M = (\Delta m_{31}^2)^M L / 4E_\nu$ ,  $\Delta_A = AL / 4E_\nu$  being  $\theta_{13}^M$  and  $(\Delta m_{31}^2)^M$ , the effective reactor mixing angle  $\theta_{13}$  and atmospheric mass-squared difference  $\Delta m_{31}^2$  in matter, with  $A$  given by  $A(\text{eV}^2) = 0.76 \times 10^{-4} \rho(\text{g/cm}^3) E_\nu(\text{GeV})$ . For antineutrinos, we replace  $A \rightarrow -A$ . As we have already discussed, the scalar-field interaction parameter,  $\eta$ , enters in as an average over the oscillation frequency mediated by the atmospheric mass-squared splitting  $\Delta m_{31}^2$  as shown in Eq. (17), in a similar way as in the electron neutrino appearance channel. For the relevant neutrino oscillation parameters in this channel (including matter effects), we follow the same specifications as the electron neutrino appearance channel.

<sup>3</sup> We have verified that our results do not significantly change by using the best-fit values from Ref. [82].

<sup>4</sup> Regarding the muon-neutrino sample, a detailed physics reach from the muon disappearance channel is not presented in the ESS $\nu$ SB CDR [37], our simulation is based on the results from Sec. 3.2 of [36].

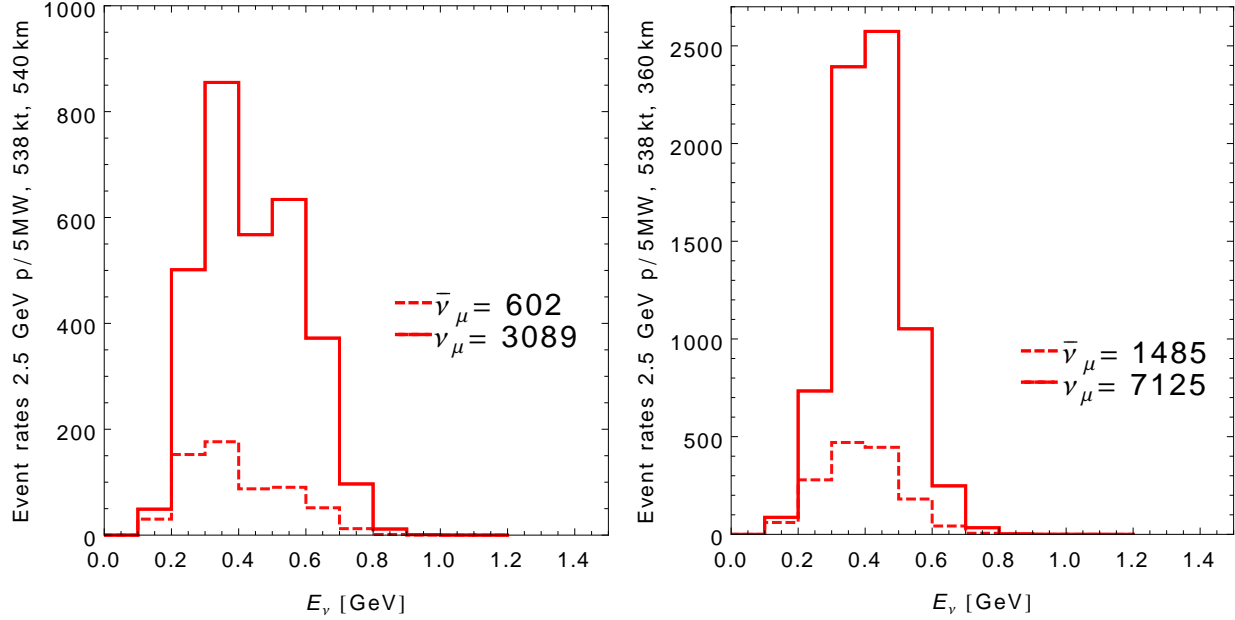


Figure 2: Expected muon-neutrino and antineutrino disappearance ( $\nu_\mu/\bar{\nu}_\mu$ ) event rates per year for an ESS $\nu$ SB setup using the neutrino oscillation parameters as given in [36], the left panel displays the baseline option of placing the detector at a distance of  $L=540$  km and the right panel for  $L=360$  km baseline case.

In Fig. 2, we display our expected signal events as a function of the neutrino energy, assuming one year of exposure, for both neutrinos and anti-neutrinos. The left panel is for the option of placing the detector at a baseline of 540 km from the source, and the right panel represents the baseline option at 360 km from the source.

Baseline run	$\nu_\mu(\bar{\nu}_\mu)$ sig.	$\bar{\nu}_\mu(\nu_\mu) \rightarrow \bar{\nu}_\mu(\nu_\mu)$	NC bckg.
360 km $\nu$	7125	54	87
( $\bar{\nu}$ )	1485	132	13
540 km $\nu$	3089	27	38
( $\bar{\nu}$ )	602	67	6

Table II: Our expected muon-neutrino disappearance signal and background events per year for an ESS $\nu$ SB setup using the neutrino oscillation parameters as given in [36].

In Table II, the total number of events per year for signal and background in the muon-

neutrino disappearance channel is introduced for both neutrinos and antineutrinos. In our analysis, we consider only the  $\bar{\nu}_\mu(\nu_\mu) \rightarrow \bar{\nu}_\mu(\nu_\mu)$  and  $\nu_\mu(\bar{\nu}_\mu)$  neutral current backgrounds for positive (negative) polarity, respectively, since they are the main contributions to this channel. As a result, there is essentially no background interference in the muon-neutrino disappearance channel.

### C. Scalar-field sensitivity

In this subsection, we introduce our results of the ULSF searches via neutrino oscillations at the ESS $\nu$ SB from the combined analysis at both appearance and disappearance channels. We have already stated that the disappearance channel will give a more restrictive result for this kind of search due to its higher statistics. Still, we include in our analysis both the electron appearance as well as the muon disappearance channels, to be the most sensitive as possible.

We employ a chi-squared test to quantify the statistical significance of the ULSF sensitivity, which is given by the adding the two channels using both neutrino and anti-neutrino data sets. The  $\chi^2$  function<sup>5</sup> is given as

$$\chi^2 = \sum_{\ell} \tilde{\chi}_{\ell}^2 + \chi_{\text{prior}}^2, \quad (20)$$

where the corresponding  $\tilde{\chi}_{\ell}^2$  function for each channel  $\ell = \{\nu_\mu(\bar{\nu}_\mu) \rightarrow \nu_e(\bar{\nu}_e), \nu_\mu(\bar{\nu}_\mu) \rightarrow \nu_\mu(\bar{\nu}_\mu)\}$  in the large data size limit is given by

$$\tilde{\chi}_{\ell}^2 = \min_{\xi_j} \left[ \sum_i^{n_{\text{bins}}} \frac{\left( N_{i,\text{true}}^{3\nu} - N_{i,\text{test}}^{3\nu+\eta}(\Omega, \eta, \{\xi_j\}) \right)^2}{\sigma_{i,\text{true}}^2} + \sum_j^{n_{\text{syst.}}} \left( \frac{\xi_j}{\sigma_j} \right)^2 \right]. \quad (21)$$

The  $N_i^{3\nu}$  are the simulated events at the  $i$ th energy bin considering the standard three neutrino oscillations as a true hypothesis.  $N_i^{3\nu+\eta}$  are the computed events at the  $i$ th energy bin with the model assuming scalar field oscillations.  $\Omega = \{\theta_{12}, \theta_{13}, \theta_{23}, \delta, \Delta m_{21}^2, \Delta m_{31}^2\}$  is the set of oscillation parameters,  $\eta$  is the ULSF parameter and  $\{\xi_j\}$  are the nuisance parameters to account for the signal, background normalization, and energy calibration systematics respectively. Moreover,  $\sigma_i = \sqrt{N_i^{3\nu}}$  is the statistical error in each energy bin while  $\sigma_j$  are the

---

<sup>5</sup> More details on the implementation of the  $\chi^2$  function, systematical errors and priors in the GLoBES software [46, 47] can be found in [86].

signal, background normalization, and energy calibration errors (see Sec. III). Furthermore, implementation of external input for the standard oscillation parameters on the  $\chi^2$  function is performed via Gaussian priors

$$\chi_{\text{prior}}^2 = \sum_k^{n_{\text{priors}}} \frac{(\Omega_{k,\text{true}} - \Omega_{k,\text{test}})^2}{\sigma_k^2}, \quad (22)$$

the central values of the priors  $\Omega_k$  are set to their true or best-fit value for normal ordering [81].  $\sigma_k$  is the uncertainty on the oscillation prior, which corresponds to a  $1\sigma$  error of 5% for  $\Delta m_{21}^2$ ,  $\Delta m_{31}^2$ ,  $\theta_{12}$ , and  $\theta_{23}$ , 3% for  $\theta_{13}$ , and 10% for the leptonic  $CP$ -violating phase  $\delta$  [35], the summation index  $k$  runs over the corresponding test oscillation parameters to be marginalized.

Besides, the expected number of events at the  $i$ th energy bin is calculated as [86]

$$N_i = \frac{\mathcal{N}}{L^2} \int_{E'_i - \Delta E'_i/2}^{E'_i + \Delta E'_i/2} dE' \int_0^\infty dE \Phi_\nu(E) \sigma_\nu(E) P_{\alpha\beta}(E) K(E, E') \varepsilon(E'), \quad (23)$$

where  $E$  is the true neutrino energy,  $E'$  is the reconstructed neutrino energy,  $\Delta E'_i$  is the bin size of the  $i$ th energy bin,  $\mathcal{N}$  is a constant normalization factor that accounts for the mass-year exposure and beam power,  $L$  is the baseline distance,  $\Phi_\nu(E)$  is the energy-dependent neutrino flux,  $\sigma_\nu(E)$  is the energy-dependent cross section,  $P_{\alpha\beta}(E)$  is the neutrino-oscillation probability,  $K(E, E')$  is the energy response-model or energy-resolution of the experiment, and  $\varepsilon(E')$  is the energy-dependent efficiency. Moreover, the neutrino-oscillation probability  $P_{\alpha\beta}(E) = P_{\nu_\alpha \rightarrow \nu_\beta}(E, L, \rho, \theta_{12}, \theta_{23}, \theta_{13}, \Delta m_{31}^2, \Delta m_{21}^2, \delta)$ ; the energy-resolution function, which relates the true and reconstructed neutrino energies follow a Gaussian distribution

$$K(E, E') = \frac{1}{\sqrt{2\pi}\sigma_R(E)} \exp \left\{ -\frac{(E - E')^2}{2\sigma_R^2(E)} \right\}, \quad (24)$$

where  $\sigma_R(E) = \beta \sqrt{E/\text{GeV}}$  GeV, in our case we assume  $\beta = (0.12, 0.10)$  for  $(e^-, \mu^-)$  respectively.

Furthermore,  $N_i^{3\nu} = S_i^{3\nu} + B_i^{3\nu}$ ,  $S_i^{3\nu}$ , and  $B_i^{3\nu}$  are the simulated signal and background events in each energy bin within the standard three neutrino oscillations framework, as described in Tables I, and II. They were computed according to Eq. (23) with true oscillation parameters fixed to their best-fit point for normal ordering (see Sec. IV A). In addition,  $N_i^{3\nu+\eta} = S_i^{3\nu+\eta} (1 + \xi_1 + g(E')\xi_3) + B_i^{3\nu+\eta} (1 + \xi_2 + g(E')\xi_4)$ ,  $S_i^{3\nu+\eta}$ , and  $B_i^{3\nu+\eta}$  are the corresponding signal and background events in each energy bin, assuming the model with scalar



field oscillations where  $P_{\alpha\beta}(E) \rightarrow P_{\alpha\beta}(E, \eta)$ . Likewise, the  $\{\xi_j\}$  are the nuisance parameters describing the systematic errors, where  $\xi_1$  and  $\xi_2$  account for the signal and background normalization, respectively, whereas  $\xi_3$  and  $\xi_4$  account for the signal and background energy calibration, the energy calibration function  $g(E')$  is

$$g(E') = \frac{(E'_i - \bar{E}')}{(E'_{max} - E'_{min})}, \quad (25)$$

where  $E'_i$  is the mean reconstructed energy at the  $i$ th energy bin;  $\bar{E}' = \frac{1}{2}(E'_{max} + E'_{min})$  is the median of the energy interval,  $E'_{min} = 0.1$  GeV is the minimum energy of the reconstructed energy window while  $E'_{max} = 1.3$  GeV is the maximum energy of the reconstructed energy window.

The sensitivity contours were computed based on the  $\Delta\chi^2 = \chi^2 - \chi^2_{\min}$  distribution, scanning over the test parameter pairs, either  $(\sin^2 \theta_{23}, \eta)$  or  $(\Delta m^2_{31}, \eta)$ , with the ULSF parameter  $\eta$  arising from the average modulation on the atmospheric mass-squared splitting  $\Delta\tilde{m}^2_{31}$ , as given in Eq. (17). All the remaining test oscillation parameters are marginalized over. The standard three neutrino oscillation picture is assumed as true hypothesis; the boundary of the corresponding allowed regions were determined by mapping the  $\Delta\chi^2$  to corresponding confidence levels using a  $\chi^2$ -distribution, assuming Wilks theorem for two degrees of freedom.

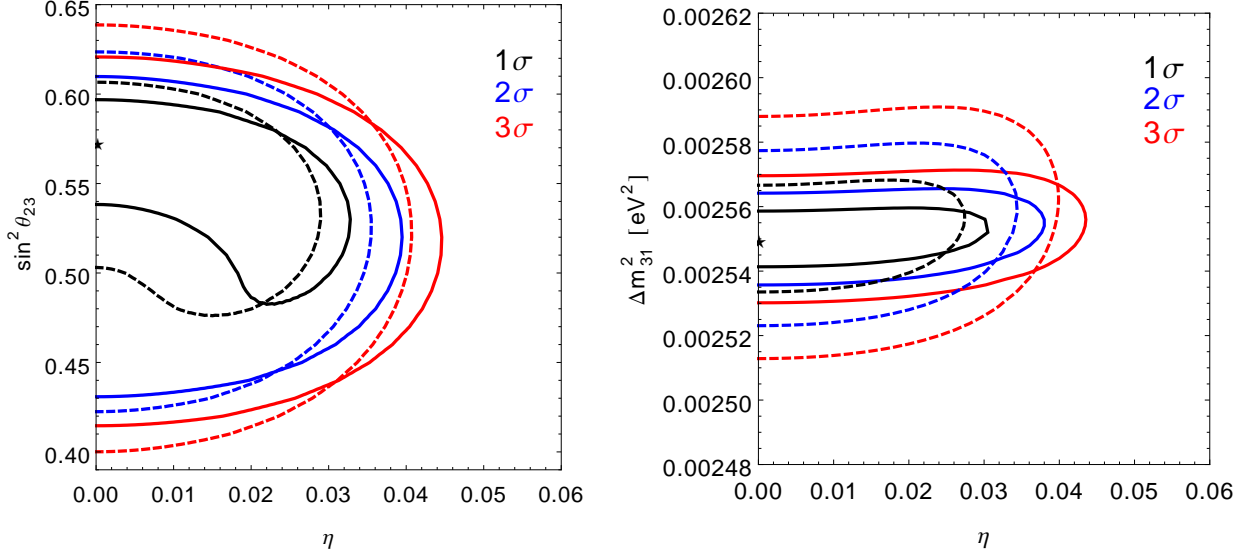


Figure 3: Expected sensitivity to the scalar field parameter  $\eta$  from the atmospheric mass squared modulation at the ESS $\nu$ SB setup; the baseline choice of  $L = 540$  km is shown in dashed lines, whereas the  $L = 360$  km in solid lines. The contours inside the black, blue, and red lines are the sensitivities at  $1\sigma$ ,  $2\sigma$ , and  $3\sigma$ , respectively.

In Fig. 3, we show our sensitivities to the scalar field scenario. The left panel displays the expected sensitivity to the ULSF in the  $(\eta, \sin^2 \theta_{23})$  plane, whereas the right panel shows the expected sensitivity in the  $(\eta, \Delta m_{31}^2)$  plane, respectively. The contours inside the black, blue, and red lines are the sensitivities at  $(1\sigma, 2\sigma, \text{ and } 3\sigma)$ , which correspond to  $\Delta\chi^2 = (2.3, 6.18, \text{ and } 11.83)$  accordingly. The star in the  $\eta - \sin^2 \theta_{23}$  and  $\eta - \Delta m_{31}^2$  planes represent the best-fit point used in the simulated data under the true hypothesis. The solid lines assume an ESS $\nu$ SB setup with a baseline of  $L = 360$  km, while the dashed lines represent a baseline of  $L = 540$  km.

We observe that the impact of the normalization systematic error is relevant for the  $L = 540$  km baseline, mainly due to a decrease in the signal events, spoiling the precision on the atmospheric mixing parameters,  $\theta_{23}$  and  $\Delta m_{31}^2$ . However, the sensitivity to the scalar field parameter is not considerably affected. As a result, we anticipate a ULSF parameter sensitivity of  $\eta < 0.043$  ( $0.039$ ) at  $3\sigma$  and  $\eta < 0.032$  ( $0.028$ ) at 90% confidence limit (C.L.) i.e.,  $\Delta\chi^2 = 4.61$ , at the  $L = 360$  km ( $L = 540$  km) baselines. Besides, the allowed values at  $3\sigma$  for the mixing angle are  $0.41 \lesssim \sin^2 \theta_{23} \lesssim 0.62$ , and for the atmospheric mass-squared

difference  $2.53 \times 10^{-3} \text{ eV}^2 \lesssim \Delta m_{31}^2 \lesssim 2.57 \times 10^{-3} \text{ eV}^2$ , at the  $L = 360 \text{ km}$  baseline option, while at the  $L = 540 \text{ km}$  baseline, the allowed values at  $3\sigma$  are  $0.40 \lesssim \sin^2 \theta_{23} \lesssim 0.64$  and  $2.51 \times 10^{-3} \text{ eV}^2 \lesssim \Delta m_{31}^2 \lesssim 2.59 \times 10^{-3} \text{ eV}^2$ .

We can notice the relevance of the expected sensitivity found here by comparing it with other studies for different types of neutrino physics. For instance, for solar neutrino experiments, it has been pointed out [20] that an order  $\mathcal{O}(10\%)$  anomalous modulation on the neutrino fluxes, due to an ultralight ( $m_\phi \sim 10^{-22} \text{ eV}$ ) scalar coupling with neutrinos could happen at solar neutrino experiments. This result translates into a bound to the scalar field parameter of  $\eta \sim 0.1$ . In addition, a projected sensitivity of  $\eta \sim 1.5\%$  and  $\eta \sim 7.5\%$  via  $\Delta m_{31}^2$  smearing are expected at the JUNO and DUNE experiments, respectively [22]. Furthermore, bounds due to the modulations from the mass-squared splitting  $\Delta m_{31}^2$  have been recently studied in Ref. [26], reporting a  $1\sigma$  sensitivity to the  $\eta$  parameter for different neutrino experiments, such as Daya Bay; with a scalar field bound of  $\eta \sim 0.08$  from the electron antineutrino disappearance channel. Similarly, the JUNO experiment is projected to be sensitive to  $\eta \sim 0.005$ , and from the electron neutrino appearance channel, a  $\eta \sim 0.01$  bound is expected for both DUNE and Hyper-Kamiokande, respectively. Regarding DUNE, the authors of Ref. [25] obtained a  $1\sigma$  sensitivity of  $\eta \sim 0.035$ . Hence, compared to our projected  $1\sigma$  sensitivities to the ULSF parameter at the ESS $\nu$ SB setup of  $\eta \sim 0.03$  from the  $L = 360 \text{ km}$  baseline option and  $\eta \sim 0.027$  from the  $L = 540 \text{ km}$  baseline, competitive bounds on the ULSF parameter can be achieved. Consequently, we expect that with the inclusion of the muon-neutrino disappearance data set, we can motivate to extend the main physics program at the ESS $\nu$ SB to search for this type of physics.

#### D. Some cosmological implications of the neutrino-ULSF interaction

Before finishing this section, we would like to discuss some important characteristics and details of the scalar field in cosmology –they can be relevant when interpreting our results.

We start this subsection by noticing, as stated in Ref [20], that the  $\hat{y}\phi$  contribution in Eq. (9) will induce quantum corrections<sup>6</sup> to the ULSF potential

$$V_\phi = \frac{m_\phi^2}{2}\phi^2 + \hat{y}n_\nu\phi + \mathcal{O}(\hat{y}^2) + \dots \quad (26)$$

---

<sup>6</sup> The tadpole contribution vanishes for off-diagonal couplings where  $\text{Tr}[m_\nu \hat{y}_{ij}] = 0$  in flavor space [26].

This contribution will produce a shift of the  $\phi$  vacuum expectation value (VEV) that goes as  $\hat{y}n_\nu\phi$ , where  $n_\nu$  is the neutrino number density. This shift could jeopardize the features of the ULSF as dark matter since the VEV of  $\phi$  will be displaced at  $T \sim \text{GeV}$ ,

$$\langle -\phi \rangle \sim \frac{\hat{y}n_\nu}{m_\phi^2} \sim 10^{21} \text{ GeV} \left( \frac{\hat{y}}{10^{-40}} \right) \left( \frac{n_\nu}{0.1 \text{ GeV}^3} \right) \left( \frac{10^{-22} \text{ eV}}{m_\phi} \right). \quad (27)$$

For this reason, it is important to consider that the temperature associated with the phase transition that sets the initial conditions for the ULSF field it is well below 1 MeV [20].

If  $\phi$  begins to oscillate at  $T_{\text{osc}} \sim \sqrt{M_{\text{Pl}} m_\phi} (m_\phi/10^{-22} \text{ eV}) \sim \text{keV}$  [10], around this temperature, the redshift  $z_{\text{osc}} \sim 2 \times 10^6$  and the average density  $\rho_\phi(z) \sim 10^{-5} \rho_{\phi,\odot} (1+z)^3$ . Thus, the scalar-field amplitude  $\phi_{\text{keV}}(z = 2 \times 10^6) \simeq 10^{26} \text{ eV} \simeq 10^{17} \text{ GeV}$ . From the sensitivity to the ULSF parameter  $\eta \sim 0.01$  at ESS $\nu$ SB, using Eq. (14) we obtain  $\hat{y} \sim 10^{-23} (m_\phi/10^{-22} \text{ eV})$  at present time. However if the coupling  $\hat{y}$  remains unmodified back to the oscillation temperature, the VEV of the scalar field ( $\langle -\phi \rangle = \phi_{\text{min}}$ ) is

$$\langle -\phi \rangle \sim \frac{\hat{y}n_\nu}{m_\phi^2} \sim 10^{20} \text{ GeV} \left( \frac{\hat{y}}{10^{-23}} \right) \left( \frac{n_\nu}{10^{-19} \text{ GeV}^3} \right) \left( \frac{10^{-22} \text{ eV}}{m_\phi} \right), \quad (28)$$

thus,  $\phi_{\text{min}} \sim 10^3 \phi_{\text{keV}}$  (which requires a coupling  $\hat{y} \lesssim 10^{-27} (m_\phi/10^{-22} \text{ eV})$  to avoid large corrections to the neutrino mass, well below the sensitivity of any terrestrial neutrino oscillation experiment). Furthermore, the contributions to the neutrino mass are  $\hat{y}\phi_{\text{keV}} \simeq 10^3 \text{ eV}$  and  $\hat{y}\phi_{\text{min}} \simeq 10^6 \text{ eV}$ , hence the effective neutrino mass at this temperature would be  $\tilde{m}(t) \simeq 10^6 \text{ eV}$ .

On the other hand, around matter-radiation equality where  $T_{\text{eq}} \sim 1 \text{ eV}$ ; the potential  $\hat{y}\phi \sim 10^{-23} \times 10^{22} \text{ eV} \sim 0.1 \text{ eV}$  and  $\hat{y}(\phi + \phi_{\text{min}}) \sim 0.11 \text{ eV}$ . Besides, the effective neutrino mass  $\tilde{m}(t) \simeq m_\nu + \hat{y}(\phi + \phi_{\text{min}})$ , assuming a bare neutrino mass  $m_\nu \sim 0.1 \text{ eV}$  we obtain  $\tilde{m}(t) \simeq 0.21 \text{ eV}$ , which is within the limit of the CMB constraint  $\sum_i m_i < 0.23 \text{ eV}$  [87]. Therefore, without invoking any model realization, unless the temperature associated with the phase transition of the ULSF occurs after matter-radiation equality (say at  $T \sim m_\nu \sim 0.1 \text{ eV}$ ), strong constraints apply to the neutrino-ULDM scenario at ESS $\nu$ SB. Moreover, if this transition happens after the formation of the CMB, the ULSF can only constitute a fraction of the DM [22]. Therefore, in our analysis for the ESS $\nu$ SB, we can consider the scalar field as being a component of the dark matter, or to be just an ultralight scalar field without participating of the DM components [88].

In the case that the phase transition can happen at temperatures of the order of 10 MeV, there could be potential contributions to the effective number of neutrino species  $N_{\text{eff}}$  during

big bang nucleosynthesis (BBN). In this scenario, the interaction term  $\hat{y}\phi$  could increase  $N_{\text{eff}}$  during BBN. However, the density of thermal neutrinos may have dominated the ULSF potential throughout this epoch, modifying Eqs. (5) and (6).

For instance, within the scenario of active-sterile mixing [31] where  $\hat{y} \approx \sin^2 \theta g$ , a potential  $g\phi_\odot \sim 10^{-7}$  eV ( $g/10^{-22})(10^{-18}\text{eV}/m_\phi)$  is able to maintain  $\Delta N_{\text{eff}} \lesssim 10^{-2}$ , increasing the potential will further reduce the contribution to  $\Delta N_{\text{eff}}$ . From the sensitivity to the ULSF parameter  $\eta \sim 0.01$  at ESS $\nu$ SB, we obtain a similar potential  $g\phi_\odot \sim 10^{-7}$  eV ( $(\hat{y}/10^{-23})(0.1/\sin^2 \theta)(10^{-18}\text{eV}/m_\phi)$ ). Therefore, we do not expect a restriction from BBN in this scenario. Other constraints from BBN can be found in Refs. [30, 89–91].

On the other hand, the CMB observations constrain the sum of the neutrino masses  $\sum_i m_i \lesssim 0.23$  eV [87]; for modulations via  $\Delta m_{31}^2$ , according to [22], this implies  $\eta(z=0) \lesssim 9 \times 10^{-3}$  ( $m_\phi/10^{-22}\text{eV}$ ), which is in good agreement with the ESS $\nu$ SB sensitivity,  $\eta(z=0) \lesssim 0.01$ .

Within the CMB era, there could be an important case to consider for us. If the potential  $\hat{y}\phi$  dominates over the neutrino bare mass terms, the neutrino mass will significantly change. The relevant neutrino mass states  $\nu_1, \nu_3$  will have the contribution [20]

$$m_{1,3}(t) \simeq \hat{y}_{1,3} \langle \phi \rangle \simeq \frac{2\hat{y}_{1,3}\sqrt{2\rho_\phi}}{\pi m_\phi}. \quad (29)$$

The CMB bound on the neutrino masses <sup>7</sup> implies a restriction for the coupling,  $\hat{y}_{1,3}^{\text{CMB}}(z=0) \lesssim 6 \times 10^{-21}$  ( $m_\phi/10^{-22}\text{eV}$ ). As we have mentioned, ESS $\nu$ SB will be sensitive to the phenomenological parameter  $\eta$  [Eq. (14)] at the percent level,

$$\eta_\Delta \propto \hat{y}_i \sqrt{\rho_\phi}/m_\phi. \quad (30)$$

This means that, for our usual choice of values  $m_\phi$  and  $\rho_\phi$ , the sensitivity to the coupling  $\hat{y}_{1,3}^{\text{CMB}}(z=0)$  would be at least one order of magnitude smaller than the ESS $\nu$ SB sensitivity.

The previous discussions assume that the ULSF accounts for all the DM in the Universe ( $\rho_\phi = \rho_{\text{DM},\odot}$ ). This may not be the case, and the ULSF could be only a fraction of this DM. The main phenomenological parameter,  $\eta$ , includes the DM density and would imply that  $\hat{y}_{1,3} \propto \eta/\sqrt{\rho_\phi}$ , if the  $\phi$  accounts for less than 20% of the total DM

---

<sup>7</sup> Recently, fits using the CMB and LSS data sets give a constraint  $\sum_i m_i \lesssim 0.40$  eV [92] that would imply a weaker restriction on  $\hat{y}_{1,3}$ .

density [33]; the scalar field amplitude  $\phi_0$  decreases by a factor of two, thus the coupling  $\hat{y}_{1,3} \gtrsim 2 \times 10^{-23} (\eta/0.01)(m_\phi/10^{-22} \text{ eV})$ . Therefore, in this scenario, the sensitivity to  $\hat{y}_{1,3}$  will be weaker. On the other hand, for the local DM density  $\rho_{\text{DM},\odot} \simeq 0.3 - 0.6 \text{ GeV/cm}^3$ ; for  $\rho_\phi = \rho_{\text{DM},\odot}$ , the coupling can vary between the range  $\hat{y}_{1,3} \simeq [1/\sqrt{2} - 1] \times 10^{-23} (\eta/0.01)(m_\phi/10^{-22} \text{ eV})$ .

Notice that, since  $\hat{y}_{1,3} \propto \eta m_\phi$ , a larger ULSF mass will reduce the sensitivity on the coupling  $\hat{y}_{1,3}$  for fixed density  $\rho_\phi$ . However, most observational features of a ULSF as DM favor a mass range  $m_\phi \sim (10^{-1} - 10) \times 10^{-22} \text{ eV}$  [4–8, 10, 12–16, 65, 66, 74].

Finally, we might worry about the thermalization of the ULSF at distant past via  $\nu\phi \rightarrow \nu\phi$  scatterings, which can lead to equilibrium among neutrinos and the ULSF. Nevertheless, the elastic scattering cross section for a scalar self-conjugate field, such as the ULSF with active neutrinos, via a spin one-half fermion  $N$  ( $M_N \gg m_\phi$ ) exchange is zero [93].<sup>8</sup>

## V. CONCLUSIONS

The dark matter problem is one of the main puzzles in physics, and different solutions have been proposed over the years. The existence of dark matter has been a strong motivation to explore alternative physical models and interactions to understand all its physical consequences ranging from particle physics to cosmology. In particular, the scalar field dark matter proposal is very successful at the cosmological level and deserves further exploration of its possible interactions with a Standard Model particle.

In this paper, we have discussed in detail the implications of a hypothetical interaction between neutrinos and an ULSF, as well as the case where this field is a DM candidate. We focused in the case of the long-baseline neutrino experiment at the ESS $\nu$ SB. As already discussed, a broad set of proposals considers either modifying of gravitational interactions or new particles at different mass scales. We have focused on the case of an ultralight scalar field and its hypothetical interaction with neutrinos. In this scenario, a modification in the expected oscillation pattern in long baseline neutrinos is expected. This modification could affect either the-neutrino mixing angles or mass-squared differences. The ESS $\nu$ SB is sensitive to the ULSF via modulations on the atmospheric mass squared difference  $\Delta m_{31}^2$ .

We found that sensitivities to the main parameter modeling the interaction between the

---

<sup>8</sup> For the scenario discussed in Ref. [30], thermalization can be avoided.

ULSF and neutrinos are:  $\eta < 0.043$  (0.039) at  $3\sigma$  and  $\eta < 0.032$  (0.028) at 90% C.L., from the  $L = 360$  km and ( $L = 540$  km) baselines, respectively. Our bounds are comparable to other long-baseline searches of this parameter. For instance, in Ref. [22], a projected sensitivity of  $\eta \sim 1.5\%$  and  $\eta \sim 7.5\%$  via  $\Delta m_{31}^2$  smearing are expected at JUNO and DUNE experiments, respectively. Projected  $1\sigma$  sensitivities of  $\eta \sim 0.035$  at DUNE [25] and  $\eta \sim 0.01$  [26] at both DUNE and Hyper-Kamiokande were also reported in the literature. Regarding reactor neutrino experiments,  $1\sigma$  sensitivities of  $\eta \sim 0.08$  from Daya Bay and  $\eta \sim 0.005$  from JUNO are reported [26]. All these bounds are comparable to our  $1\sigma$  sensitivities to the ULSF parameter at the ESS $\nu$ SB setup, namely  $\eta \sim 0.03$  from the  $L = 360$  km baseline option and  $\eta \sim 0.027$  from the  $L = 540$  km baseline. Therefore, the incorporation of the muon-neutrino disappearance sample will not only benefit precision measurements at ESS $\nu$ SB [36] but also opens a window to search for scalar-field modulations from the atmospheric mass-squared splitting  $\Delta m_{31}^2$ .

The ESS $\nu$ SB experiment represents an opportunity to measure the leptonic  $CP$ -violating phase accurately. Besides, it will allow searching for different types of new physics at a competitive level. The case of the ULSF candidate is an example of this potential.

### ACKNOWLEDGMENTS

This work was partially supported by SNI-México and CONACyT research Grant No. A1-S-23238. Additionally the work of R.C. was partially supported by COFAA-IPN, Estímulos al Desempeño de los Investigadores (EDI)-IPN and SIP-IPN Grants No. 20210704 and No. 20221329. We thank the anonymous referee for the illuminating comments, especially on the cosmological implications of the neutrino-ULSF interaction.

- 
- [1] V. Sahni and L.-M. Wang, Phys. Rev. D **62**, 103517 (2000), astro-ph/9910097.
  - [2] W. Hu, R. Barkana, and A. Gruzinov, Phys. Rev. Lett. **85**, 1158 (2000), astro-ph/0003365.
  - [3] T. Matos, F. S. Guzman, and L. A. Urena-Lopez, Class. Quant. Grav. **17**, 1707 (2000), astro-ph/9908152.
  - [4] T. Matos and L. A. Urena-Lopez, Class. Quant. Grav. **17**, L75 (2000), astro-ph/0004332.
  - [5] A. Arbey, J. Lesgourgues, and P. Salati, Phys. Rev. D **65**, 083514 (2002), astro-ph/0112324.

- [6] A. Arbey, J. Lesgourgues, and P. Salati, *Phys. Rev. D* **64**, 123528 (2001), astro-ph/0105564.
- [7] J. Magana and T. Matos, *J. Phys. Conf. Ser.* **378**, 012012 (2012), 1201.6107.
- [8] A. Suárez, V. H. Robles, and T. Matos, *Astrophys. Space Sci. Proc.* **38**, 107 (2014), 1302.0903.
- [9] D. J. E. Marsh, *Phys. Rept.* **643**, 1 (2016), 1510.07633.
- [10] L. Hui, J. P. Ostriker, S. Tremaine, and E. Witten, *Phys. Rev. D* **95**, 043541 (2017), 1610.08297.
- [11] J.-W. Lee, *EPJ Web Conf.* **168**, 06005 (2018), 1704.05057.
- [12] L. A. Ureña López, *Front. Astron. Space Sci.* **6**, 47 (2019).
- [13] T. Matos, A. Vazquez-Gonzalez, and J. Magana, *Mon. Not. Roy. Astron. Soc.* **393**, 1359 (2009), 0806.0683.
- [14] I. Rodriguez-Montoya, J. Magana, T. Matos, and A. Perez-Lorezana, *Astrophys. J.* **721**, 1509 (2010), 0908.0054.
- [15] J. Lesgourgues, A. Arbey, and P. Salati, *New Astron. Rev.* **46**, 791 (2002).
- [16] A. Arbey, J. Lesgourgues, and P. Salati, *Phys. Rev. D* **68**, 023511 (2003), astro-ph/0301533.
- [17] T. Harko, *Mon. Not. Roy. Astron. Soc.* **413**, 3095 (2011), 1101.3655.
- [18] V. H. Robles and T. Matos, *Mon. Not. Roy. Astron. Soc.* **422**, 282 (2012), 1201.3032.
- [19] J.-W. Lee and S. Lim, *JCAP* **01**, 007 (2010), 0812.1342.
- [20] A. Berlin, *Phys. Rev. Lett.* **117**, 231801 (2016), 1608.01307.
- [21] V. Brdar, J. Kopp, J. Liu, P. Prass, and X.-P. Wang, *Phys. Rev. D* **97**, 043001 (2018), 1705.09455.
- [22] G. Krnjaic, P. A. N. Machado, and L. Necib, *Phys. Rev. D* **97**, 075017 (2018), 1705.06740.
- [23] J. Liao, D. Marfatia, and K. Whisnant, *JHEP* **04**, 136 (2018), 1803.01773.
- [24] D. Kim, P. A. N. Machado, J.-C. Park, and S. Shin, *JHEP* **07**, 057 (2020), 2003.07369.
- [25] A. Dev, P. A. N. Machado, and P. Martínez-Miravé, *JHEP* **01**, 094 (2021), 2007.03590.
- [26] M. Losada, Y. Nir, G. Perez, and Y. Shpilman, *JHEP* **04**, 030 (2022), 2107.10865.
- [27] Y. Zhao, *Phys. Rev. D* **95**, 115002 (2017), 1701.02735.
- [28] Y. Farzan, *Phys. Lett. B* **797**, 134911 (2019), 1907.04271.
- [29] J. M. Cline, *Phys. Lett. B* **802**, 135182 (2020), 1908.02278.
- [30] A. Dev, G. Krnjaic, P. Machado, and H. Ramani (2022), 2205.06821.
- [31] G.-y. Huang, M. Lindner, P. Martínez-Miravé, and M. Sen, *Phys. Rev. D* **106**, 033004 (2022), 2205.08431.



- [32] M. Losada, Y. Nir, G. Perez, I. Savoray, and Y. Shpilman (2022), 2205.09769.
- [33] T. Kobayashi, R. Murgia, A. De Simone, V. Iršič, and M. Viel, Phys. Rev. D **96**, 123514 (2017), 1708.00015.
- [34] N. Bar, K. Blum and C. Sun, Phys. Rev. D **105**, no.8, 8 (2022), 2111.03070.
- [35] E. Baussan et al. (ESSnuSB), Nucl. Phys. B **885**, 127 (2014), 1309.7022.
- [36] A. Alekou et al. (ESSnuSB), Eur. Phys. J. C **81**, 1130 (2021), 2107.07585.
- [37] A. Alekou et al. (2022), 2206.01208.
- [38] L. Agostino, M. Buizza-Avanzini, M. Dracos, D. Duchesneau, M. Marafini, M. Mezzetto, L. Mosca, T. Patzak, A. Tonazzo, and N. Vassilopoulos (MEMPHYS), JCAP **01**, 024 (2013), 1206.6665.
- [39] S. Kumar Agarwalla, S. S. Chatterjee, and A. Palazzo, JHEP **12**, 174 (2019), 1909.13746.
- [40] M. Ghosh, T. Ohlsson, and S. Rosauero-Alcaraz, JHEP **03**, 026 (2020), 1912.10010.
- [41] S. Choubey, M. Ghosh, D. Kempe, and T. Ohlsson, JHEP **05**, 133 (2021), 2010.16334.
- [42] R. Majhi, D. K. Singha, K. N. Deepthi, and R. Mohanta, Phys. Rev. D **104**, 055002 (2021), 2101.08202.
- [43] M. Blennow, M. Ghosh, T. Ohlsson, and A. Titov, JHEP **07**, 014 (2020), 2004.00017.
- [44] S. S. Chatterjee, O. G. Miranda, M. Tórtola, and J. W. F. Valle (2021), 2111.08673.
- [45] Y. H. Ahn, S. K. Kang, R. Ramos, and M. Tanimoto (2022), 2205.02796.
- [46] P. Huber, M. Lindner, and W. Winter, Comput. Phys. Commun. **167**, 195 (2005), hep-ph/0407333.
- [47] P. Huber, J. Kopp, M. Lindner, M. Rolinec, and W. Winter, Comput. Phys. Commun. **177**, 432 (2007), hep-ph/0701187.
- [48] B. Carr and F. Kuhnel, Ann. Rev. Nucl. Part. Sci. **70**, 355 (2020), 2006.02838.
- [49] B. Carr, F. Kuhnel, and L. Visinelli, Mon. Not. Roy. Astron. Soc. **506**, 3648 (2021), 2011.01930.
- [50] A. Arbey and F. Mahmoudi, Prog. Part. Nucl. Phys. **119**, 103865 (2021), 2104.11488.
- [51] L. Di Luzio, M. Giannotti, E. Nardi, and L. Visinelli, Phys. Rept. **870**, 1 (2020), 2003.01100.
- [52] K. Arun, S. B. Gudennavar, and C. Sivaram, Adv. Space Res. **60**, 166 (2017), 1704.06155.
- [53] M. Drewes, Int. J. Mod. Phys. E **22**, 1330019 (2013), 1303.6912.
- [54] K. C. Y. Ng, B. M. Roach, K. Perez, J. F. Beacom, S. Horiuchi, R. Krivonos, and D. R. Wik, Phys. Rev. D **99**, 083005 (2019), 1901.01262.

- [55] E. Oks, *New Astron. Rev.* **93**, 101632 (2021), 2111.00363.
- [56] M. Milgrom, *Astrophys. J.* **270**, 365 (1983).
- [57] T. Baker et al., *Rev. Mod. Phys.* **93**, 015003 (2021), 1908.03430.
- [58] L. Randall and R. Sundrum, *Phys. Rev. Lett.* **83**, 3370 (1999), hep-ph/9905221.
- [59] L. Randall and R. Sundrum, *Phys. Rev. Lett.* **83**, 4690 (1999), hep-th/9906064.
- [60] D. Clowe, M. Bradac, A. H. Gonzalez, M. Markevitch, S. W. Randall, C. Jones, and D. Zaritsky, *Astrophys. J. Lett.* **648**, L109 (2006), astro-ph/0608407.
- [61] A. A. Klypin, A. V. Kravtsov, O. Valenzuela, and F. Prada, *Astrophys. J.* **522**, 82 (1999), astro-ph/9901240.
- [62] B. Moore, S. Ghigna, F. Governato, G. Lake, T. R. Quinn, J. Stadel, and P. Tozzi, *Astrophys. J. Lett.* **524**, L19 (1999), astro-ph/9907411.
- [63] P. J. E. Peebles and A. Nusser, *Nature* **465**, 565 (2010), 1001.1484.
- [64] A. P. Lundgren, M. Bondarescu, R. Bondarescu, and J. Balakrishna, *Astrophys. J. Lett.* **715**, L35 (2010), 1001.0051.
- [65] T. Matos and L. A. Urena-Lopez, *Phys. Rev. D* **63**, 063506 (2001), astro-ph/0006024.
- [66] A. Suarez and T. Matos, *Mon. Not. Roy. Astron. Soc.* **416**, 87 (2011), 1101.4039.
- [67] A. Arvanitaki, S. Dimopoulos, S. Dubovsky, N. Kaloper, and J. March-Russell, *Phys. Rev. D* **81**, 123530 (2010), 0905.4720.
- [68] M. Cicoli, V. Guidetti, N. Righi, and A. Westphal, *JHEP* **05**, 107 (2022), 2110.02964.
- [69] T. Bernal, L. M. Fernández-Hernández, T. Matos, and M. A. Rodríguez-Meza, *Mon. Not. Roy. Astron. Soc.* **475**, 1447 (2018), 1701.00912.
- [70] L. A. Ureña López, V. H. Robles, and T. Matos, *Phys. Rev. D* **96**, 043005 (2017), 1702.05103.
- [71] R. Hlozek, D. Grin, D. J. E. Marsh, and P. G. Ferreira, *Phys. Rev. D* **91**, 103512 (2015), 1410.2896.
- [72] N. Bar, D. Blas, K. Blum and S. Sibiryakov, *Phys. Rev. D* **98**, no.8, 083027 (2018), 1805.00122.
- [73] A. Arvanitaki, J. Huang, and K. Van Tilburg, *Phys. Rev. D* **91**, 015015 (2015), 1405.2925.
- [74] L. A. Urena-Lopez, in *4th Mexican School of Astrophysics* (2007), pp. 295–302.
- [75] P. F. de Salas, K. Malhan, K. Freese, K. Hattori, and M. Valluri, *JCAP* **10**, 037 (2019), 1906.06133.
- [76] P. F. de Salas and A. Widmark, *Rept. Prog. Phys.* **84**, 104901 (2021), 2012.11477.

- [77] S. Sivertsson, J. I. Read, H. Silverwood, P. F. de Salas, K. Malhan, A. Widmark, C. F. P. Laporte, S. Garbari, and K. Freese, *Mon. Not. Roy. Astron. Soc.* **511**, 1977 (2022), 2201.01822.
- [78] J.-E. Campagne, M. Maltoni, M. Mezzetto, and T. Schwetz, *JHEP* **04**, 003 (2007), hep-ph/0603172.
- [79] M. Blennow, E. Fernandez-Martinez, T. Ota, and S. Rosauero-Alcaraz, *Eur. Phys. J. C* **80**, 190 (2020), 1912.04309.
- [80] H. Nunokawa, S. J. Parke, and J. W. F. Valle, *Prog. Part. Nucl. Phys.* **60**, 338 (2008), 0710.0554.
- [81] P. F. de Salas, D. V. Forero, S. Gariazzo, P. Martínez-Miravé, O. Mena, C. A. Ternes, M. Tortola, and J. W. F. Valle, *JHEP* **02**, 071 (2021), 2006.11237.
- [82] I. Esteban, M. C. Gonzalez-Garcia, M. Maltoni, T. Schwetz, and A. Zhou, *JHEP* **09**, 178 (2020), 2007.14792.
- [83] S. K. Agarwalla, S. Choubey, and S. Prakash, *JHEP* **12**, 020 (2014), 1406.2219.
- [84] K. Chakraborty, S. Goswami, C. Gupta, and T. Thakore, *JHEP* **05**, 137 (2019), 1902.02963.
- [85] S. Choubey and P. Roy, *Phys. Rev. D* **73**, 013006 (2006), hep-ph/0509197.
- [86] P. Huber, M. Lindner, and W. Winter, *Nucl. Phys. B* **645**, 3 (2002), hep-ph/0204352.
- [87] P. A. R. Ade et al. (Planck), *Astron. Astrophys.* **594**, A13 (2016), 1502.01589.
- [88] F. Capozzi, I. M. Shoemaker and L. Vecchi, *JCAP* **07**, 004 (2018), 1804.05117.
- [89] N. Blinov, K. J. Kelly, G. Z. Krnjaic, and S. D. McDermott, *Phys. Rev. Lett.* **123**, 191102 (2019), 1905.02727.
- [90] G.-y. Huang, T. Ohlsson, and S. Zhou, *Phys. Rev. D* **97**, 075009 (2018), 1712.04792.
- [91] J. Venzor, A. Pérez-Lorenzana, and J. De-Santiago, *Phys. Rev. D* **103**, 043534 (2021), 2009.08104.
- [92] C. S. Lorenz, L. Funcke, M. Löffler, and E. Calabrese, *Phys. Rev. D* **104**, 123518 (2021), 2102.13618.
- [93] C. Boehm and P. Fayet, *Nucl. Phys. B* **683**, 219 (2004), hep-ph/0305261.